CERN-ACC-2019-028
04 February 2019

Search for heavy resonances at the FCC-hh

C. Helsens[1)*], D. Jamin[†], M. Selvaggi[*]

On behalf of the FCC-hh Collaboration

[*] *CERN EP-Departement, CH-1211 Geneva 23, Switzerland,* [†] *Academia Sinica, Institute of Physics, Taipei, Taiwan*

Abstract

This paper explores the physics reach of the proton-proton Future Circular Collider (FCC-hh) for searches of new particles decaying to two high energetic leptons, jets (non-tops), tops and W/Z boson. We discuss the expected exclusion limits and discovery potential for benchmark models predicting new massive particles that result in resonant structures in the invariant mass spectrum. The study is based on the Madgraph5 and Pythia8 Monte Carlo generators using large event statistics for the FCC running conditions.

This work was carried out in the framework of the FCC-hh Collaboration

[1] corresponding.author@cern.ch

1. Introduction

Particle accelerators are built to answer some of the most fundamental questions about the natural world. For LHC it was guaranteed that the Standard Model (SM) Higgs boson would be found; however, for the next generation of machines there is no possibility to guarantee that any new particle will be discovered. Still with much higher center of mass energies compared to LHC, there are guaranteed deliverables like the study of the Higgs and top-quark properties and exploration of electroweak symmetry breaking phenomena with unmatchable precision and sensitivity.

New machines are built to make direct discoveries, and even though we do not have any guaranted discoveries, we need to make sure that we will cover a large fraction of Beyond the SM (BSM) phase space. Qualitatively, the mass reach should roughly scale by a factor of $\sqrt{s}/14$, so ~ 7 for FCC at $\sqrt{s} = 100\,\text{TeV}$However, with the parton luminosities evolving with Q^2, thus dropping a bit faster at high energy, one typically finds it is only a factor of ~ 5 increase. But the statistics are also enhanced by several orders of magnitude for many Beyond Standard Model (BSM) phenomena, that the LHC could barely touch during its exploitation. It is not only that the mass reach increases by a large factor, but it is the fact that if the LHC were to see some hints of possible new physics, by increasing the energy by a factor seven, we would increase the statistics by two or even three orders of magnitude, and we can use this new machine to study with great accuracy what it is that has been found. In addition we could have the ability to provide firm answers to questions such as: is the SM dynamics all there at the TeV scale, is there a TeV scale solution to the hierarchy problem, is dark matter a thermal wimp (either we discover it as a WIMP, or we find out DM is not a WIMP and it has to be something else), was the cosmological EW phase transition 1^{st} order, etc...

Concerning the topic of this paper, the discovery potential for new resonances not predicted by the SM makes Future Circular Colliders (FCC) the only place to search directly for such heavy particles, compared to the current LHC and the coming HL-LHC. In the framework of FCC it is also extremely relevant to discuss the main limitations of the detector in identifying high energetic top-quarks or W/Z bosons. Indeed 100 TeV proton-proton collisions will produce very large quantities of multi-TeV's bosons or top, thus the design of the detector needs detailed optimisations in order to achieve the required physics goals. The capabilities of such a detector should include the capabilities of measuring multi-TeV leptons, top-quarks and bosons, and will be discussed in this paper.

This document presents the expectations of some of the most relevant BSM scenarios and the considered models are discussed in the section 2. Details on the generators, detector parameterization, statistical methods and other analysis techniques developed are presented in the section 3. The leptonic resonances (ee, $\mu\mu$, $\tau\tau$) and the hadronic resonances (WW, $t\bar{t}$ and jj) analyses are detailed in sections 4 and 5 respectively.

2. BSM Models

In order to explore and contrast the capabilities of future colliders to discover and examine the properties of new physics, a broad set of benchmark models needs to be employed. In the case of new heavy resonances, this benchmark set should be sufficiently complete such that all of the major discovery channels of relevance are represented. As discussed above, here we are particularly interested in the 2-body final states of these resonances (since they are generally dominant in almost all new physics scenarios) consisting of opposite sign dilepton pairs ($e^+e^-, \mu^+\mu^-$ and $\tau^+\tau^-$), dijets, $t\bar{t}$ and W^+W^-. We note that it is highly likely that at least one or possibly more of these 2-body channels will posses a respectable branching fraction for the new resonances that result from any specific beyond the Standard Model scenario. Note that decays into pairs of secondary objects that then themselves decay hadronically can often populate the dijet channel if the final state jets are sufficiently boosted so this channel can represent many different final states unless substructure studies are performed. When there are 2 or more

of these channels available for simultaneous study we have an increased chance of learning significantly more about the underlying physics model behind the new resonance. The most important properties of a newly discovered resonance that need to be determined (other than the mass) are its production cross section, which will sometimes require a good understanding of the underlying background shape especially for a broad resonance and its spin (as was the case in the example of the Higgs boson). These properties alone can provide important information about the BSM model from which the signal originated. The spin measurement usually requires the reconstruction of the angular distribution of the resonance decay products and, hence, a respectable amount of statistics although the observation of certain final states can immediately exclude some spin possibilities as was the case with $H \to \gamma\gamma$.

A new, neutral, spin-1 gauge boson, Z', which is usually a color-singlet object produced in the $q\bar{q}$ channel, is a ubiquitous feature of many models that predict new physics [1–4]. While falling into several distinct classes, Z' are most commonly associated with the extension of the the SM electroweak gauge group by an additional U(1) or SU(2) factor although more significant augmentations are possible. When the additional factor is non-abelian, as in the case of SU(2), a new $W^{\pm}$' gauge boson generally also appears in the spectrum together with the Z' and with a comparable mass. Of this subset of models, those that arise from Grand Unified Theory frameworks are the ones most commonly encountered in the literature and include familiar examples such as the Left-Right Symmetric Model (LRM) [5, 6] which results from SO(10) (or larger GUT groups) and where the SM is augmented by an $SU(2)_R$ factor. Most simply, the LRM can arise, e.g., from SO(10) GUT breaking directly to $SU(2)_L \times SU(2)_R \times U(1)_{B-L}$ which then breaks to the SM at the few to multi-TeV scale. A second set of GUT-based Z' models arise from E_6 [7–10] where most simply $E_6 \to \mathrm{SM} \times U(1)_\psi \times U(1)_\chi \to \mathrm{SM} \times U(1)_\theta$, where a new $U(1)_\theta$ gauge group factor is predicted. Note here θ labels the remaining linear combination of $U(1)_\psi$-$U(1)_\chi$ that remains unbroken to lower energies (in comparison to the GUT scale). A common set of features of this GUT-based model class include their possesing generation-universal couplings of the Z' to the SM fermions, their charges commuting with those of the SM so that, e.g., u_L and d_L have the same Z' coupling and the resonances themselves are usually narrow, reflecting electroweak strength or weaker couplings with width to mass ratios $\Gamma/M < 0.01 - 0.03$. In particular, the GUT origin of these models implies that this class of Z' can be used to simultaneously study all of the dileptonic channels: e^+e^-, $\mu^+\mu^+$ as well as $\tau^+\tau^-$ together with the dijets and boosted $t\bar{t}$ channels as well.

With this much information potentially available from the observation of a given Z' in multiple channels one may try to distinguishable it from others of similar type given sufficient statistics and well-controlled systematics. In addition to relative cross section measurements, e.g., that of dijets and/or $t\bar{t}$ compared to dileptons, the cleanliness of the dilepton channel itself can allow us to obtain additional information. Since the leptons can be signed, their angular distribution allows us to determine their forward-backward asymmetry, A_{FB}, (defined in the dilepton center of mass frame) which depends upon the quark and lepton couplings of the Z' in a different manner than does the dilepton production cross section and, hence, will differ from model to model. Note that theoretically the scattering angle is usually defined as the one between the outgoing negatively charged lepton and the incoming valence quark direction which is usually also the direction of the boost of the center of mass frame as seen in the lab frame. However, sometimes this condition does not hold and the anti-quark direction is instead that of the boost and this must be corrected for statistically in Monte Carlo, but not an an event-by-event basis. This observable is discussed more fully below along with some of its alternative definitions. A second possibility [11] is to make use of the fact that the rapidity distributions of the $u\bar{u}$ and $d\bar{d}$ PDFs are somewhat different. Since various Z' will generally couple differently to the u and d quarks the rapidity distributions of the dilepton final state will probe these coupling variations. This possibility can be probed by forming the rapidity ratio, r_y, which is the ratio of the number of central dilepton pairs to that at larger rapidities; this too will be discussed in further detail below.

Returning to our discussion of these specific GUT-inspired models, we note that in the LRM with the assumption of left- and right-handed gauge couplings, i.e., $\kappa = g_R/g_L = 1$, all of the various interactions

of the Z' with the SM fields are completely fixed. However, in the E_6 model case, the single new mixing parameter, θ, controls the couplings of the Z' to the various SM particles; four particular choices for the value of this parameter correspond to the more specific model cases discussed here and are denoted as ψ, χ, η and I. As in the SM, the Z' in GUT models generally couple to all the familiar quarks and leptons and thus can easily populate simultaneously the various fermionic 2-body final states listed above at various predictable rates. The measurement of these rates (as well as other associated observables) can be then used to discriminate among the various Z' possibilities after discovery as will be discussed further below. Note that the decay rate for Z' into the W^+W^- final state in GUT frameworks is highly dependent on the details of the model building assumptions within a specific scenario and especially upon the detailed nature of spontaneous symmetry breaking as manifested by the amount of mixing (if it occurs at all) between the Z' and SM Z; the Z' coupling to W^+W^- in U(1) extensions is always controlled solely by the amount of this gauge boson mixing.

The Z' of the Sequential Standard Model [12] is often included within this GUT class of models although it is not a true gauge theory in the conventional sense. However, it has been used very frequently for many years as a standard candle by experimenters since it conveniently posits the existence of heavier copies of the usual SM gauge bosons with exactly the same couplings as do the gauge bosons in the SM; this provides a useful yardstick with which one can make comparisons easily.

Alternative models of electroweak symmetry breaking, including the topcolor assisted technicolor scenarios, can also frequently lead to Z'-like states [13] that can produce resonance signatures. The greatest difference of such theories from the GUT-type Z' model class lies in their having generation-dependent couplings of potentially QCD strength. (The color-octet versions of such states in this model class are called colorons.) This implies that the corresponding resonance will likely not be narrow and will preferentially couple, by construction, to the third generation, e.g., the highly boosted $t\bar{t}$ final state, thus proving another useful benchmark model for this channel. Similar new Z' states can also arise in Little Higgs models [14] which can also have preferential decays to third generation states.

Occasionally the expected properties of a new Z' models are completely data-driven. A Z' with an unusual flavor-dependent coupling structure has been suggested as a (partially complete) UV model to explain the apparent anomaly seen in semileptonic $b \to s l^+ l^-$ decays [15, 16]. In effective field theory language, a new interaction of the form $\sim \bar{b} P_L s \bar{\mu} P_L \mu$ of proper strength can provide a reasonable fit to these experimental observations [17] which can be the result of the exchange of a very heavy Z' potentially accessible to high energy colliders [18]. This Z', in the weak basis, couples only to the third generation quark doublet and to the muon lepton doublet so that it will have a suppressed production cross section at hadron colliders. Such a Z' could be observed in both the dimuon and ditop channels.

Models of composite quarks and leptons offer another path wherein new resonances are predicted. Excited quarks [19, 20], Q^*, are spin-1/2, color triplet objects which carry the same SM quantum numbers as do the SM quarks. Here one imagines that the usual quarks have some type of internal structure and are held very tightly together by some new BSM force; these constituents when excited in some way yield the more massive states we would then observe as Q^*. There is, as of yet, no fundamental, UV-complete model encompassing this idea so that this framework is purely phenomenological. The SM quarks couple to these excited states via a magnetic dipole-like interaction together with an associated gauge boson such as the gluon or the SM W, Z or γ. This interaction is suppressed by a large 'compositeness scale', Λ, since it corresponds to a dim-6 operator, and the relative coupling strengths to the different gauge bosons are partially controlled by a set of essentially free parameters, f_i. Excited quarks can be singly produced in the gq channel to which they will also dominantly decay due to the presence of the strong coupling constant, yielding the dijet signature of interest to us here although decays into, e.g, the $q\gamma$ channel are also of some interest. It is useful to have a benchmark model with dijet decays which take place in the gq channel (as opposed to a Z' which can only populate the $q\bar{q}$ dijet channel) with which to compare and contrast. The angular distributions of the 2 jets in the dijet decay, which will require significant statistics to determine, can provide us information about the spin of the original

resonance and the nature of its couplings to the decay products [21–24].

Spin-2 graviton resonances occur in extra-dimensional scenarios that attempt to address the hierarchy problem, in particular, in the case of the warped extra dimensional model of Randall and Sundrum (RS) [25]. In such setups, the SM gauge fields and fermions are generally allowed to propagate in the 5-D bulk [26–30] whereas electroweak symmetry breaking occurs on or near the TeV/SM brane via the usual Higgs mechanism. This approach simultaneously helps to address the SM fermion mass hierarchy by the localization properties of the SM fermions in the bulk. One finds that, due to the shape of their 5-D wavefunctions, the Kaluza-Klein excitations of the familiar graviton, G_{RS} [31] will dominantly decay into objects localized near to where SM symmetry breaking occurs, i.e., Higgs boson pairs and $t\bar{t}$ as well as to the longitudinal components of the massive SM gauge bosons, e.g., $W_L^+W_L^-$, all with relatively fixed branching factions with only some small allowed variations. Thus $G_{RS} \to W^+W^-$ in the RS framework provides an excellent benchmark model for the study of resonant W-pairs which are also quite highly boosted. If these W's decay hadronically, given this high boost, this final state may also (appear to) populate the resonant dijet channel. One notes that apart from the G_{RS} mass scale itself, essentially the only other free parameter in this RS model setup (wherein the lighter fermions are essentially decoupled from the graviton resonances), is frequently denoted by $c = k/\bar{M}_{Pl}$, which simply controls the overall coupling strength to all of the various SM particles.

3. Simulation setup

3.1. Monte-Carlo production

Monte Carlo (MC) simulated event samples are used to simulate the response of the detector to signal and backgrounds. Signals are generated with PYTHIA8 [32] version v8.201 with the `NNPDF2.3NNLO` PDF set [33] using the leading order cross-section from the generator with no k-factor. The SM backgrounds are Drell-Yan, di-jet (QCD), top pairs ($t\bar{t}$), VV and V + jets where $V = W/Z$, were generated using MG5_aMC [34] v2.5.5 at leading order only with the `NNPDF3.0NLO` [33] PDF set in bins of H_T. A k-factor of 2 is applied to all the background processes to account for higher order corrections and is considered to be very conservative.

3.2. Simulation of the detector response

This study discusses the discovery potential of heavy resonances decaying to multi-TeV final states. The ability to accurately reconstruct highly boosted final states is largely dependent on the nature of the object and on the detector assumptions. Generally speaking, the energy-momentum resolution of calorimetric objects such as electrons, photons and jets improves as a function of the energy. Conversely, the momentum resolution of charged particles reconstructed as tracks decrease with the momentum as the curvature of the trajectory vanishes. In addition, at high energies, composite objects such as jets, or hadronically decaying τ's and heavy bosons tend to be highly collimated. This results in an effectively coarser granularity of the detector, which can potentially limit the ability to resolve and identify the decay products inside the jets, thereby limiting the identification and QCD background rejection capabilities.

The detector response has been simulated via the DELPHES software package [35]. For the $\sqrt{s} = 100\,\text{TeV}$ collider, the reference FCC-hh detector configuration has been used as a baseline [36, 37]. Hereafeter, we will simply refer to FCC-hh detector and will only discuss detector specifications that are relevant for high p_{T} objects. The overall contribution of pile-up is neglected altogether, as it is assumed to have a relative negligible impact of multi-TeV objects.

3.2.1. Tracking

After collision, parton showering, hadronisation, and decays, the first step of DELPHES is the propagation of long-lived particles inside the tracking volume within a uniform axial magnetic field parallel to the beam direction. The magnetic field strength B, the size of the tracking radius L and the single hit spatial resolution $\sigma_{r\phi}$ are the main parameters that determine the resolution on the track transverse momentum:

$$\frac{\sigma(p_{\mathrm{T}})}{p_{\mathrm{T}}} \approx \frac{\sigma_{r\phi}\ p_{\mathrm{T}}}{B \cdot L^2}. \tag{1}$$

These specifications of the FCC-hh detector would allow measurements of $p_{\mathrm{T}} = 1$ TeV charged hadrons with a precision of $\sigma(p_{\mathrm{T}})/p_{\mathrm{T}} \simeq 2\%$.

Central, isolated, high momentum charged hadrons tracks are assumed to be reconstructed with an efficiency $\varepsilon = 95\%$. However, charged particles confined inside a highly boosted jet can be extremely collimated, resulting in unresolvable tracker hits, especially in the innermost tracking layers. Although an accurate description of this feature would require a full event reconstruction by means of a GEANT-based simulation [38], a specific DELPHES module aimed at reproducing this has been designed. Whenever two or more tracks fall within an angular separation $\sigma(\eta,\phi)$, only the highest momentum track is reconstructed. This effect can result in an additional inefficiency to that shown in Table 1, and can affect the ability to reconstruct tracks in the core of highly boosted jets, as shown in Figure 1 (left).

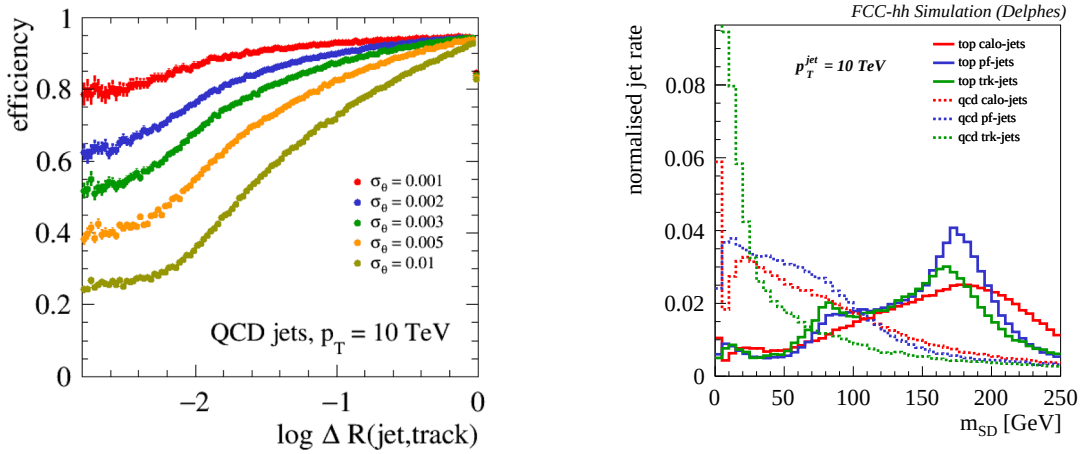

Figure 1: Left: Track reconstruction efficiency inside highly QCD boosted jets as function of the angular distance ΔR between the track and the center of the jet for different assumptions on the tracker spatial resolution. Right: Reconstructed "soft-dropped" jet mass of highly boosted top and QCD jets with various sets of input to the jet clustering algorithm: tracks only, calorimeters towers only and particle-flow candidates.

Muons are also reconstructed using tracking. However, an additional stand-alone muon measurement is provided by the angular difference between track angle in the muon system and the radial line connection to the beam axis, giving a large improvement on the resolution at high p_{T} [36]. Again, assuming a 2 times better position resolution of in the muon system for the FCC-hh detector, a combined muon momentum resolution of $\sigma(p_{\mathrm{T}})/p_{\mathrm{T}} \simeq 5\%$ can be achieved for momenta as high as $p_{\mathrm{T}} = 15$ TeV/c.

3.2.2. Calorimetry and Particle-Flow

After propagating within the magnetic field, long-lived particles reach the electromagnetic (ECAL) and hadronic (HCAL) calorimeters. Since these are modeled in DELPHES by two-dimensional grids of variable spacing, the calorimeter deposits natively include finite angular resolution effects. Separate grids for

	FCC-hh
$B_z\ (T)$	4
Length (m)	10
Radius (m)	1.5
ε	0.95
$\sigma(\eta,\phi)$	1 mrad
$\sigma(p_T)/p_T$ (tracks)	$0.02 \cdot p_{\mathrm{T}}$ (TeV/c)
$\sigma(p_T)/p_T = 5\%$ (muons) $p_{\mathrm{T}} = 15$ TeV	

Table 1: Tracking-related parameters for the FCC-hh detector in Delphes.

ECAL and HCAL have been designed for the FCC-hh detector in order to accurately model the angular resolution on reconstructed jets. The energy resolution of the calorimeters is assumed to be the same for both detectors.

In DELPHES the information provided by the tracker and calorimeters is combined within the particle-flow algorithm for an optimal event reconstruction. If the momentum resolution of the tracking system is better than the energy resolution of calorimeters (typically for momenta below some threshold) the charged particles momenta are measured mainly through tracking. Vice-versa at high energy, calorimeters provide a better momentum measurement. The particle-flow algorithm exploits this complementarity to provide the best possible single charged particle measurement — the *particle-flow tracks*. These contain electron, muons and charged hadrons. Jet collections are then formed using several different input objects such as tracks (*Track-jets*), calorimeter (*Calo-jets*) and particle-flow candidates (*PF-jets*). The Delphes framework integrates the FastJet package [39], allowing for jet reconstruction with the most popular jet clustering algorithms. In the present study the anti-k_T algorithm [40] is used with several jet clustering R parameters ($R = 0.2, 0.4, 0.8, 1.5$).

Common jet shape observables used for jet substructure analysis such as N-subjettiness [41] and the soft-dropped mass [42] are computed on-the-fly and stored in the output jet collections. As an illustration, the reconstructed soft-dropped mass in the FCC-hh detector for top and QCD jets with $p_{\mathrm{T}} = 10$ TeV and cone size $R = 0.2$ is shown in Figure 1(right). Thanks to the superior tracker segmentation, we find *Track-jets* to perform better in terms of QCD background rejection despite the slightly worse jet mass resolution.

	FCC-hh
$\sigma(E)/E$ (ECAL)	$10\%/\sqrt{E} \oplus 1\%$
$\sigma(E)/E$ (HCAL)	$50\%/\sqrt{E} \oplus 3\%$
$\eta \times \phi$ cell size (ECAL)	(0.01×0.01)
$\eta \times \phi$ cell size (HCAL)	(0.025×0.025)

Table 2: Calorimeter parameters for the FCC-hh detector in Delphes.

3.2.3. Object identification efficiencies

Trigger, reconstruction and identification efficiencies are parametrised as function of the particle momentum in DELPHES. Given that these parameterisations depend on the detailed knowledge of the detector, we simply use a global parameterisation for each object.

For electron and muons, the isolation around a cone is computed as the sum of over the full list of *particle-flow candidates* within a cone R excluding the particle under consideration. No selection

on the isolation variable is applied during DELPHES processing since the optimal selection working point is analysis and object dependent. Electrons and muons originating from heavy resonances are highly boosted and populate the central rapidity region of the detector. For the purpose of this study flat reconstruction identification efficiencies are assumed (see Table 3).

The identification of jets that result from τ decays or heavy flavour quarks — b or c quarks — typically involves the input from tracking information, such as vertex displacement or low level detector input such as hit multiplicity [43, 44]. Such information is not available as a default in DELPHES. Instead, a purely parametric approach based on Monte-Carlo generator information is used. The probability to be identified as b or τ depends on user-defined parameterizations(see Table 3). The behaviour of vanilla heavy flavour tagging algorithms in regimes of extreme boosts is yet unknown. We make the conservative assumption of vanishing efficiency as a function of the transverse momentum for both b and τ-jets, as shown in Table 3. This choice is motivated by the fact that decay products originating from highly boosted b and τ decays will be extremely collimated and highly displaced, making their reconstruction difficult.

	electrons	muons	photons	b-jets	τ-jets
FCC-hh	99%	95%	95%	(1 - p_{T} [TeV]/15)·85%	(1 - p_{T} [TeV]/30)·60%

Table 3: Global reconstruction efficiency of high p_{T} central objects for the FCC-hh detector in Delphes.

A mis-tagging efficiency, that is, the probability that a particle other than b or τ be wrongly identified as a b or a τ has been included in the simulation and assumes a similar falling behaviour as a function of the jet momentum. For the b-tagging, the mistag efficiency are parameterised separately for light-jets (uds-quarks) and c-jets. For the $\tau-$tagging we consider only mis-identification from QCD jets. Table 4 summarises the main values for the mis-tagging efficiency.

	light (b-tag)	charm (b-tag)	QCD (τ-tag)
FCC-hh	(1 - p_{T} [TeV]/15)·1%	(1 - p_{T} [TeV]/15)·5%	(8/9 - p_{T} [TeV]/30)·1%

Table 4: Mis-identification efficiency of high p_{T} central heavy flavour jets for the FCC-hh detector in Delphes.

3.3. Treatment of the Monte-Carlo samples

The modelling of the backgrounds in the high tagging regimes is a challenging task. The requirement of b tagging in some MC samples can drastically reduce the available statistics. This shortage of events that pass the b-tagging cut in the signal regime, in conjunction with the large cross section of some of the backgrounds can lead to very spiky templates. To overcome this problem the tag rate function (TRF) method is used. By using the TRF method, no event is cut based on its b-tagging count, but instead all the events are weighted. This weight can be interpreted as the probability of the given event to contain the desired number of b jets. To achieve this, the tagging efficiency (a function of η, p_{T} and true jet flavour) was used to calculate the event weight based on the kinematics and flavour of the jets found in each event. Despite the fact that very large amount of Monte-Carlo statistic has been simulated in bins of H_T and the usage of TRF to save events, there are still large statistical fluctuations from high weight events. In order to reduce this effect, and when large fluctuations are observed, the background spectrum is fitted. Further details on the TRF and fitting procedure are given in Appendix B. and C respectively.

3.4. Statistical analysis

Hypothesis testing is performed using a modified frequentist method based on a profile likelihood that takes into account the systematic uncertainties as nuisance parameters that are fitted to the expected Monte-Carlo. The full shape information is used, which help from the sidebands to reduce the effect of systematics uncertainties in the signal region. The test statistic q_μ is defined as the profile log-likelihood ratio: $q_\mu = -2\ln(\mathscr{L}(\mu,\hat{\hat{\theta}}_\mu)/\mathscr{L}(\hat{\mu},\hat{\theta}))$, where $\hat{\mu}$ and $\hat{\theta}$ are the values of the parameters that maximise the likelihood function (with the constraint $0 \leq \hat{\mu} \leq \mu$), and $\hat{\hat{\theta}}_\mu$ are the values of the nuisance parameters that maximise the likelihood function for a given value of μ. In the absence of any significant deviation from the background expectation, q_μ is used in the CL_s method [45, 46] to set an upper limit on the signal production cross-section times branching ratio at the 95% CL. For a given signal scenario, values of the production cross-section (parameterised by μ) yielding $CL_s < 0.05$, where CL_s is computed using the asymptotic approximation [47], are excluded at 95% CL. For a 5σ discovery, the quantity 1-CL_b must be smaller than $2.87 \cdot 10^{-7}$ [45] and is also computed using the asymptotic approximation.

4. Di-lepton channels

The decay products of heavy resonances are in the multi-TeV regime and the capability to reconstruct their momentum imposes stringent requirement on the detector design. In particular, reconstructing the track curvature of multi-TeV muons requires excellent position resolution and a large lever arm. In this section, the expected sensitivity is presented for a $Z' \to \ell\ell$ (where $\ell = e, \mu$) and $Z' \to \tau\tau$ separately.

4.1. The e^+e^- and $\mu^+\mu^-$ final states

Events are required to contain two isolated opposite sign leptons with $p_{\mathrm{T}} > 1$ TeV, $|\eta|$<4 and an invariant mass $m_{ll} > 2.5$ TeV. Figure 2 left shows the invariant mass for a 30 TeV Z'_{SSM} signal for the $\mu\mu$ channel. The di-electron invariant mass spectrum is not shown, but as expected from the calorimeter constant term that dominates the resolution at high p_{T}, the mass resolution is better for the ee channel. The di-lepton invariant mass spectrum is used as the discriminant and a 50% normalisation uncertainty on the background normalisation is assumed. Figure 2 (bottom left) shows the 95% CL exclusion limit obtained with $30\,\mathrm{ab}^{-1}$ of data combining ee and $\mu\mu$ channels. Figure 2 (bottom right) shows the integrated luminosity required to reach a 5σ discovery as a function of the mass of the heavy resonance. The $Z' \to$ ee and $Z' \to \mu\mu$ channel display very similar performance due to the low background rates. We conclude therefore that the reference detector design features near to optimal performance for searches involving high p_{T} muon final states. Combining ee and $\mu\mu$ channels, masses up to 42 TeV can be excluded or discovered. Event yields and limits for ee and $\mu\mu$ alone can be found in Appendix E and Appendix D respectively.

4.2. The $\tau^+\tau^-$ final state

At current LHC [48], the most sensitive channel to search for high mass di-τ resonances is when both τ leptons decays hadronically, and this is the focus of the analysis presented in this section. The event selection requires two jets with $p_T > 0.5$ TeV and $|\eta| < 2.5$, both identified as τ's. To ensure no overlap between the $\ell = e, \mu$ and τ final states, jets containing an electron or a muon with $p_{\mathrm{T}} > 100$ GeV are vetoed. Finally, requirements of $\Delta\phi(\tau_1,\tau_2) > 2$ and $2.5 < \Delta R(\tau_1,\tau_2) < 4$ are applied to suppress multi-jet background. Furthermore, mass dependent cuts are applied to maximise the signal significance and are summarised in Table 5. Several proxies for the true resonance mass have been tested, such as the invariant mass of the two τ's, with and without correction for the missing energy, but the transverse

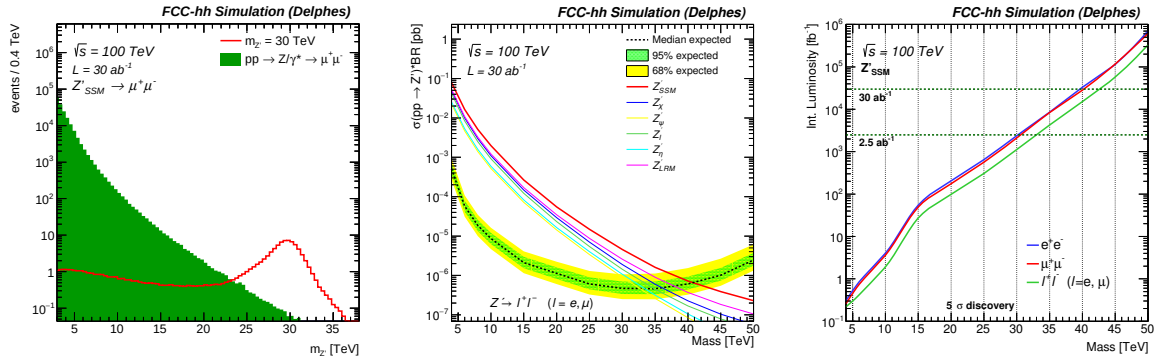

Figure 2: Left: Invariant mass for a 30 TeV signal after full event selection for the $\mu\mu$ channel. Middle: 95% CL limit versus mass for the combined di-lepton (ee, $\mu\mu$) channel. Right: integrated luminosity versus mass for a 5σ discovery comparing ee, $\mu\mu$ and combined channels.

mass [2] provided the best sensitivity and is therefore used to estimate the sensitivity. Figure 3 shows the di-τ transverse mass (left) for a 10 TeV Z'_{SSM}, the 95% CL exclusion limits for 30 ab^{-1} of data (middle) and the required integrated luminosity versus mass of the resonance to reach a 5σ discovery (right). Heavy resonance decaying to τ leptons reconstructed in the hadronic decay mode are more challenging given the overwhelming multi-jet background, but masses up to 18 TeV could be probed. The tau-tagging efficiencies considered in this analysis are assumed to be pessimistic, but only a study made in full simulation could provide realistic numbers, and should be performed in a later stage of the study.

Z' mass [TeV]	$\Delta\phi(\tau_1,\tau_2)$	$\Delta R(\tau_1,\tau_2)$	E_T^{miss}
$4-8$	>2.4	>2.5 and <3.5	>400 GeV
10	>2.4	>2.7 and <4	>300 GeV
$12-14$	>2.6	>2.7 and <4	>300 GeV
$16-18$	>2.7	>2.7 and <4	>300 GeV
>18	>2.8	>3 and <4	>300 GeV

Table 5: List of mass dependent cuts optimised to maximise the sensitivity for the $Z' \to \tau\tau$ search.

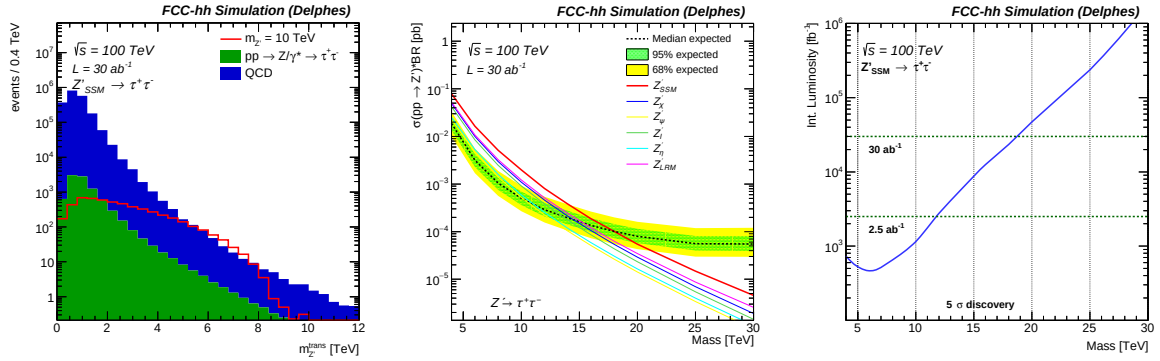

Figure 3: Left: Di-τ transverse mass for a 10 TeV signal after full event selection. Middle: 95% CL limit versus mass. Right: integrated luminosity versus mass for a 5σ discovery.

[2] the transverse mass is defined as $m_T = \sqrt{2p_{\mathrm{T}}^{Z'} * E_T^{\mathrm{miss}} * (1 - cos\Delta\phi(Z', E_T^{\mathrm{miss}}))}$

5. Hadronic final states

Heavy resonances decaying hadronically also imposes stringent requirement on the detector design. For instance, precise jet energy resolution requires full longitudinal shower containment and highly boosted top quarks and W bosons decay into highly collimated jets that need to be disentangled from standard QCD jets by studying their substructure. High discrimination power and sensitivity for these searches at such extreme energies, requires excellent granularity both in the tracking detectors and calorimeters.

5.1. Multi-Variate object tagging

An important ingredient of the hadronic searches is the identification of heavy boosted top quarks and W bosons. Two object level taggers using Boosted Decision Trees (BDT) were developed to discriminate W and top jets against the light jet flavours treated as background. Top and W taggers were optimised using jets with a transverse boost of p_{T} =10 TeV. At these extreme energies, W and top jets have a characteristic angular size $R = 0.01 - 0.02$, i.e smaller than the typical electromagnetic and hadronic calorimeter cells. Following the approach described in [49], we exploit the superior track angular resolution and reconstruct jets from tracks only using the anti-k_T algorithm with a parameter R=0.2, but also larger values are used to increase the discrimination power of the BDT. The missing neutral energy is corrected for by rescaling the track 4-momenta by the factor $p_{\mathrm{T},trk}/p_{\mathrm{T},PF}$, where $p_{\mathrm{T},trk}$ is the track Jet p_{T} and $p_{\mathrm{T},PF}$ is the Particle-Flow (PF) Jet p_{T}. In what follows, we will simply refer to "track jets" as the jet collection that includes the aforementioned rescaling. The boosted top tagger is built from jet substructure observables: the soft-dropped jet mass [42] (m_{SD}) and N-subjettiness [41] variables $\tau_{1,2,3}$ and their ratios τ_2/τ_1 (τ_{21}) and τ_3/τ_2 (τ_{32}). The W-jet tagger also uses an "isolation-like" variable that exploits the absence of high p_{T} final state-radiation (FSR) in the vicinity of the W decay products. We call these variables $E_F(n,\alpha)$ and define them as:

$$E_F(n,\alpha) = \sum_{\frac{n-1}{5}\alpha<\Delta R(k,jet)<\frac{n}{5}\alpha} p_{\mathrm{T}}^{(k)} \Bigg/ \sum_{\Delta R(k,jet)<\alpha} p_{\mathrm{T}}^{(k)} \tag{2}$$

with k running over the jet constituents and $\alpha = 0.05$. We construct 5 variables $E_F(n,\alpha)$ with $n = [1,2,3,4,5]$ and use them as input to the BDT. The W tagging performance has significantly better performance due to the good discrimination power of the energy-flow variables. We choose the working points for the analyses presented later with a top and W tagging efficiencies of $\varepsilon_S^{\mathrm{top}} = 60\%$ and $\varepsilon_S^{\mathrm{W}} = 90\%$ corresponding respectively to a background rejection of $\varepsilon_B^{\mathrm{top}} = \varepsilon_B^{\mathrm{W}} = 90\%$. These working points corresponds to a cut at 0.15 on the BDT value for both taggers. Independent samples have been generated for the training of the BDT in such a way that there is no overlap with the events used in the analysis. More details on the multi-Variate object tagging can be found in Appendix A.

5.2. The jj final state

Jets are clustered using particle-flow candidates with the anti-k_T [40] algorithm and parameter R=0.4. We require at least two very energetic jets with p_{T}>3 TeV and $|\eta| < 3$. As di-jet events from signal will tend to be more central than for background, the rapidity difference between the two leading jets $\Delta(\eta_1,\eta_2)$ is required to be smaller than 1.5. The di-jet invariant mass for the $Q^* \to jj$ signal with a mass of 40 TeV together with the QCD contribution after the full event selection is shown on Figure 4 (left). The middle Figure shows the 95% CL exclusion limit obtained with 30 ab^{-1} of data and the right Figure shows the integrated luminosity required to reach a 5σ discovery as a function of the Q* mass. For this very simple case of strongly coupled object we reach 95% CL exclusion limits of 43 TeV and 5σ discovery reach of 40 TeV with 30 ab^{-1} of integrated luminosity.

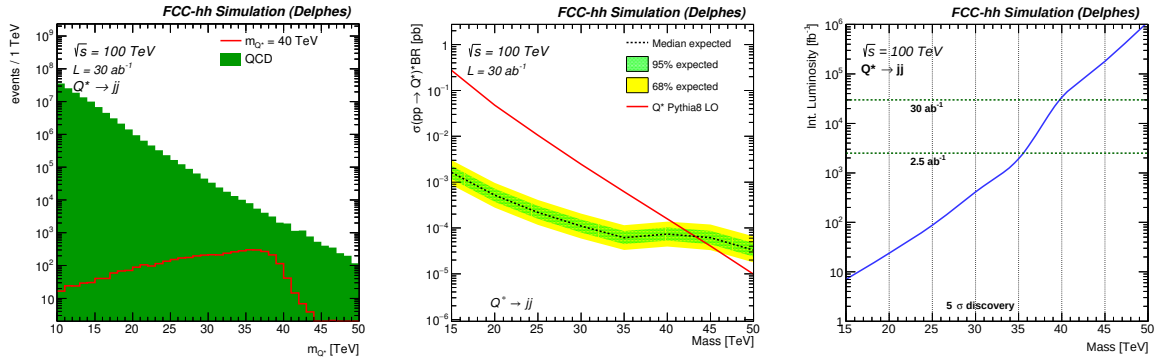

Figure 4: Invariant mass distribution of the two selected jets for a 40 TeV signal (left), 95% CL limit versus mass (middle) and 5σ discovery reach (right).

5.3. The $t\bar{t}$ final state

To resolve the jet sub-structure, track jets are found to perform better compared to particle-flow jets, thus the $G_{RS} \to W^+W^-$ and $Z' \to t\bar{t}$ searches are using track jets. As no lepton veto is applied, there is also some acceptance for leptonic decays and the sensitivity to semi-leptonic or $t\bar{t}$ decays is enhanced by adding the $\vec{p}_{\mathrm{T}}^{\,\mathrm{miss}}$ vector to the closest jet 4-momentum (among the two leading jets). We require two jets with a p_{T}>3 TeV and $|\eta| < 3$ and $\Delta(\eta_1, \eta_2) < 2.4$. Both jets must be top tagged (section 5.1) by requiring multivariate tagger score larger than 0.15. In addition, the two selected high-p_{T} jets must be tagged as b-jets. Finally, to further reject QCD, we require for both jets the soft-dropped mass to be larger than 40 GeV. Figure 5 (right) shows the di-top invariant mass distribution after the final cuts for a 20 TeV signal. Thanks to the BDT discriminant, the largest background contribution is top pair production and the QCD contribution is now the second leading one. The middle Figure shows the 95% CL exclusion limit obtained with 30 ab^{-1} of data and the right Figure shows the integrated luminosity required to reach a 5σ discovery as a function of the Z' mass. Further developments to improve the mass resolution could be considered to improve the sensitivity, but already with such wide spectrum, exclusions between 25 and 28 TeV and discoveries between 18 and 24 TeV are reached depending on the model (Z'_{SSM}or leptophobic Z'_{TC2}).

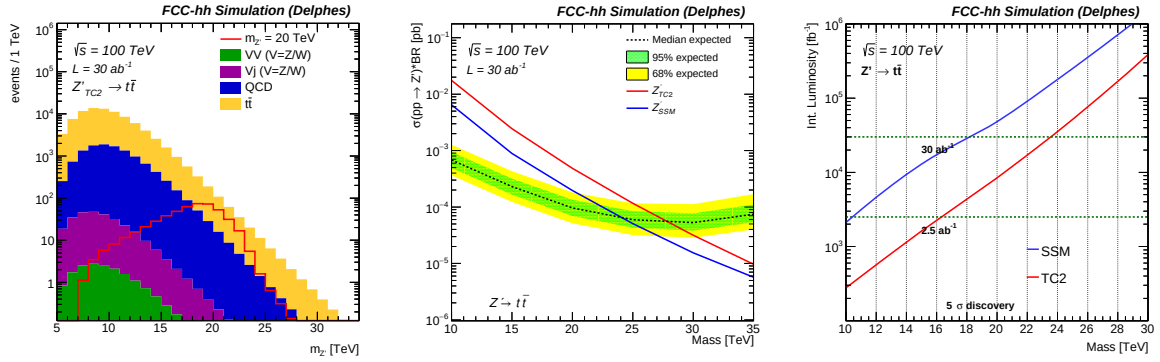

Figure 5: Invariant mass distribution of the two selected top-jets (left) for a 20 TeV signal (left), 95% CL limit versus mass (middle) and 5σ discovery reach (right).

5.4. The W^+W^- final state

The event selection consists of two jets with a p_T>3 TeV, $|\eta| < 3$ and $\Delta(\eta_1, \eta_2) < 2.4$. Both jets must be W tagged (section 5.1) by requiring multivariate tagger score larger than 0.15. Finally, to further reject QCD, we require for both jets the soft-dropped mass to be larger than 40 GeV. Figure 6 (right) shows the di-boson invariant mass distribution after the final cuts for a 20 TeV signal. Given the very good performance of the BDT discriminant, the QCD contribution is greatly reduced. The middle Figure shows the 95% CL exclusion limit obtained with 30 ab^{-1} of data and the right Figure shows the integrated luminosity required to reach a 5σ discovery as a function of the Randall-Sundrum Graviton mass. Further developments to improve the W-jet/QCD could be considered to improve the sensitivity as well as combining with leptonic channels, but already with the current assumptions, exclusion of 28 TeV and discovery of 22 TeV is obtained.

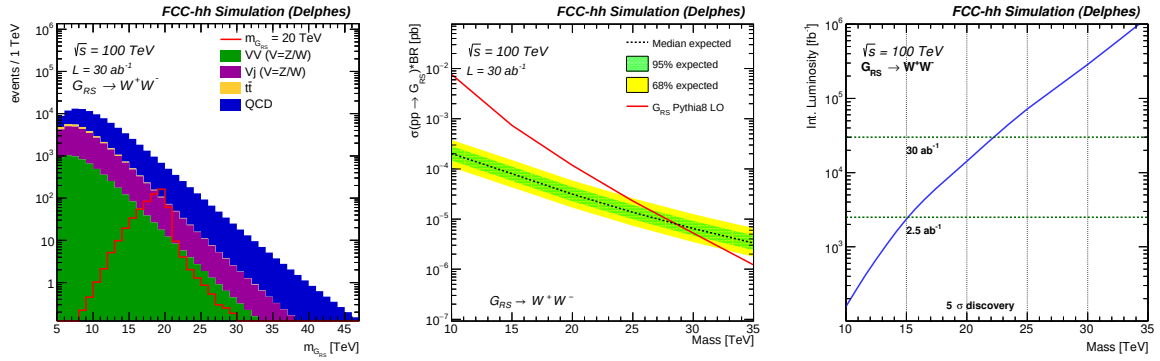

Figure 6: Invariant mass distribution of the two selected W-jets for a 20 TeV signal (left), 95% CL limit versus mass (middle) and 5σ discovery reach (right).

6. Conclusion

This paper presents studies of a search for heavy resonances decaying to leptons, bosons, top or light quarks in the context of energy frontier colliders.

A. Multivariate object tagger

The training samples are built from jets that do not contain leptons, for example from sem-leptonic b-decays. The BDT parameters used are the following : NTrees=600, MaxDepth=4, AdaBoost, AdaBoostBeta=0.15, SeparationType=GiniIndex, nCuts=100, PruneMethod=NoPruning. As an example, the $E_F(n = 1, \alpha = 0.05)$ observable is shown in Figures 7 left. The evolution of the light jet efficiency versus the W and top tagging efficiencies for both taggers is shown in Figure 7 right. Cross-checks have been performed to further validate the procedure. First, by removing highly correlated variables, such as **CH - @David Add example**, it showed the same performances **CH - @ David, then why don't we remove the correlated variables?**. As a second test, the BDT response has been tested for different signal masses to understand how the mass dependence could affect the analyses. For the cut used in the analysis (BDT score greater than 0.15), the shape of the BDT is not dramatically changing the signal efficiency.

The input variables used to train the BDT, ordered by training weight, can be found in table 6.

W tagger		top tagger	
variable	weight	variable	weight
τ_3 (track jet, R=0.2)	0.12	τ_1 (track jet, R=0.2)	0.21
m_{SD} (track jet, R=0.2)	0.11	m_{SD} (track jet, R=0.2)	0.17
τ_{31} (track jet, R=0.2)	0.10	τ_{31} (track jet, R=0.2)	0.11
$E_F(n=5,\alpha=0.05)$	0.09	τ_2 (track jet, R=0.2)	0.10
$E_F(n=4,\alpha=0.05)$	0.09	τ_3 (track jet, R=0.2)	0.09
$E_F(n=1,\alpha=0.05)$	0.08	m_{SD} (track jet, R=0.8)	0.09
$E_F(n=2,\alpha=0.05)$	0.07	m_{SD} (track jet, R=0.4)	0.09
$E_F(n=3,\alpha=0.05)$	0.06	τ_{32} (track jet, R=0.2)	0.08
τ_{21} (track jet, R=0.2)	0.06	τ_{21} (track jet, R=0.2)	0.06
m_{SD} (track jet, R=0.8)	0.06		
m_{SD} (track jet, R=0.4)	0.06		
τ_1 (track jet, R=0.2)	0.05		
τ_2 (track jet, R=0.2)	0.04		
τ_{32} (track jet, R=0.2)	0.02		

Table 6: Summary of the input variables to the BDT and their relative weight for both W and top taggers.

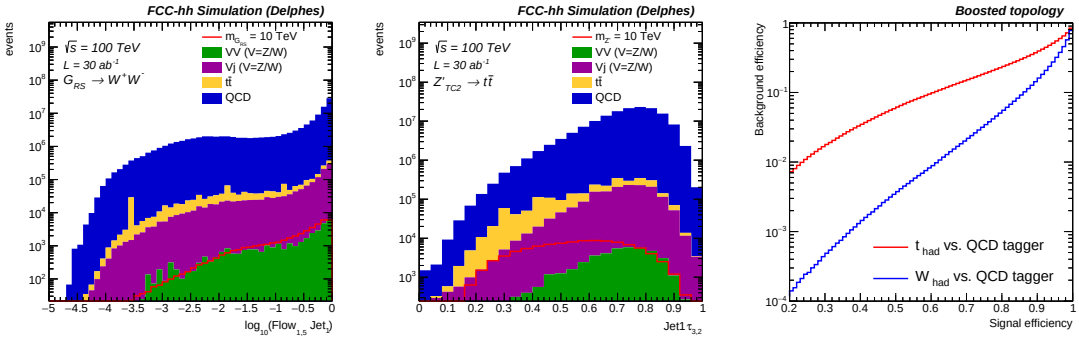

Figure 7: Left: Energy-flow ($E_F(1,0.05)$) observable for W and QCD jets. Middle: ($\tau_(3,2)$) observable for t and QCD jets. Right: Light jet rejection versus tagging efficiency for the W tagger (blue) and top tagger (red) -> re-do on-going.

B. Tagging rate function

Given a jet with η, p_{T} and flavour f, its tagging probability can be noted as:

$$\varepsilon\left(f,|\eta|,p_{\mathrm{T}}\right)$$

For a given event with N jets, its probability of containing exactly one b-tag jet can be computed as:

$$P_{=1}=\sum_{i=1}^{N}\left(\varepsilon_i\prod_{i\neq j}\left(1-\varepsilon_j\right)\right)$$

In the same way, it can be used to compute the probability for inclusive b-tag selections:

$$P_{=0}=\prod_{i=1}^{N}\left(1-\varepsilon_j\right)$$

$$P_{\geq 1}=1-P_{=0}$$

It was verify that the TRF methods agrees well with the direct tagging.

C. Background fit

$$f(z) = p_1(1-z)^{p_2} z^{p_3} z^{p_4 logz} \tag{3}$$

where $z = m_{jj}/\sqrt{s}$. This fit is used in order to have a smooth shape for the backgrounds, while the normalisation is taken prior to the fit (see figure 8).

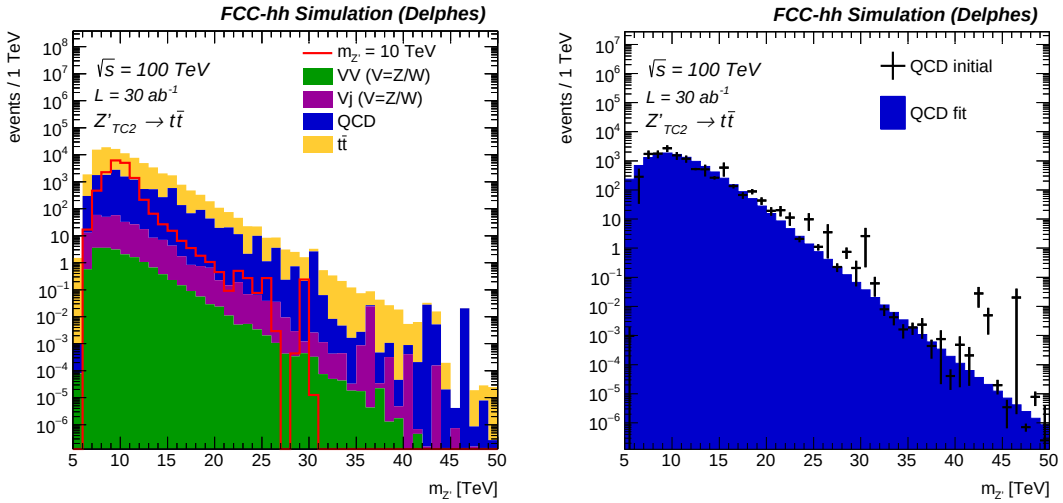

Figure 8: Invariant mass prior to fit.

D. Event yields

	ee	$\mu\mu$
Drell-Yan	206882.9	236597.9
Z' 4 TeV	1421357.9	1598969.4
Z' 6 TeV	349922.4	393117.6
Z' 8 TeV	115043.5	129698.7
Z' 10 TeV	45423.5	50873.3
Z' 20 TeV	1192.3	1411.5
Z' 30 TeV	88.2	107.6
Z' 40 TeV	11.7	14.1
Z' 50 TeV	3.2	3.7

Table 7: Expected number of events at FCC-hh for the $Z' \to ee$ and $Z' \to \mu\mu$ analysis after the full event selection for the SSM signal hypothesis and considering 30 ab^{-1} of integrated luminosity.

	di-jet		$t\bar{t}$		WW	
	pre-sel	final-sel	pre-sel	final-sel	pre-sel	final-sel
di-jet	385555434	373661126	154855591	11439.8	154856148	64484
$t\bar{t}$	-	-	1114779	74193.6	1114779	3185
di-bosons	-	-	41820	17.1	41820	6092
boson+jet	-	-	1610472	264.1	1610472	25377
total bkg	385555434	373661126	157622662	85914	154856148	99137
10 TeV	-	-	101529	15601	47853	15745
20 TeV	1253072	1239813	7774	500.6	1282	578
30 TeV	69922	67488	485.2	13.2	61.4	30.1
40 TeV	4589	4373	-	-	-	-

Table 8: Expected number of events at FCC-hh for the di-jet, $t\bar{t}$ and WW analyses after pre and final selection.

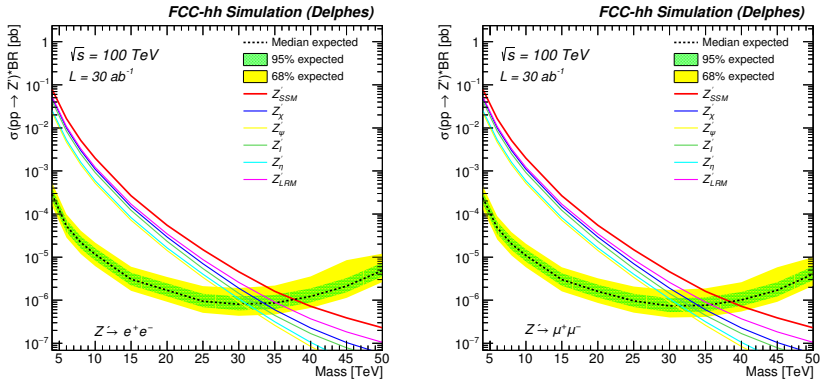

Figure 9: Limit versus mass for the ee channel (left) and $\mu\mu$ channel (right) for an integrated luminosity of 30 ab^{-1}.

E. More information on analyses

F. Summary plots

The discovery potential for the heavy resonances presented in this document are summarised in Figure 10 for FCC-hh.

References

[1] P. Langacker, *The Physics of Heavy Z' Gauge Bosons*, Rev. Mod. Phys. **81** (2009) 1199, DOI: 10.1103/RevModPhys.81.1199, arXiv: 0801.1345 [hep-ph].

[2] T. G. Rizzo, *Z' phenomenology and the LHC*, Proceedings of Theoretical Advanced Study Institute in Elementary Particle Physics : Exploring New Frontiers Using Colliders and Neutrinos (TASI 2006): Boulder, Colorado, June 4-30, 2006, 2006, p. 537, arXiv: hep-ph/0610104 [hep-ph], URL: http://www-public.slac.stanford.edu/sciDoc/docMeta.aspx?slacPubNumber=slac-pub-12129.

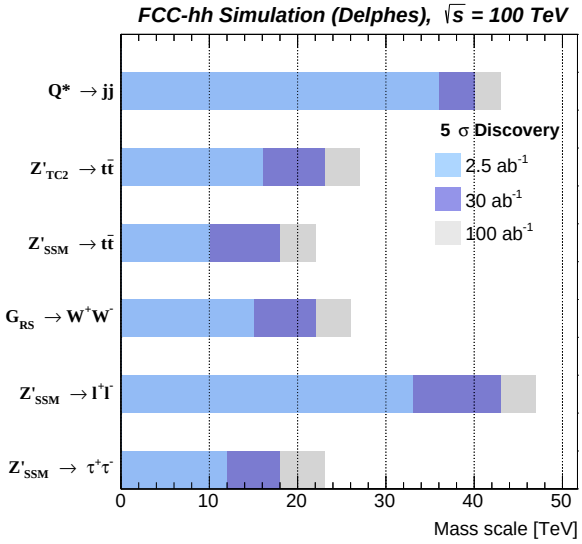

Figure 10: Summary of a 5σ discovery reach as a function of the resonance mass for different luminosity scenario of FCC-hh.

[3] M. Carena et al., *Z' gauge bosons at the Tevatron*, Phys. Rev. **D70** (2004) 093009, DOI: 10.1103/PhysRevD.70.093009, arXiv: hep-ph/0408098 [hep-ph].

[4] E. Salvioni, G. Villadoro, F. Zwirner, *Minimal Z-prime models: Present bounds and early LHC reach*, JHEP **11** (2009) 068, DOI: 10.1088/1126-6708/2009/11/068, arXiv: 0909.1320 [hep-ph].

[5] G. Senjanovic, R. N. Mohapatra, *Exact Left-Right Symmetry and Spontaneous Violation of Parity*, Phys. Rev. **D12** (1975) 1502, DOI: 10.1103/PhysRevD.12.1502.

[6] R. N. Mohapatra, G. Senjanovic, *Neutrino Masses and Mixings in Gauge Models with Spontaneous Parity Violation*, Phys. Rev. **D23** (1981) 165, DOI: 10.1103/PhysRevD.23.165.

[7] R. W. Robinett, J. L. Rosner, *Mass Scales in Grand Unified Theories*, Phys. Rev. **D26** (1982) 2396, DOI: 10.1103/PhysRevD.26.2396.

[8] D. London, J. L. Rosner, *Extra Gauge Bosons in E(6)*, Phys. Rev. **D34** (1986) 1530, DOI: 10.1103/PhysRevD.34.1530.

[9] J. L. Hewett, T. G. Rizzo, *Low-Energy Phenomenology of Superstring Inspired E(6) Models*, Phys. Rept. **183** (1989) 193, DOI: 10.1016/0370-1573(89)90071-9.

[10] A. Joglekar, J. L. Rosner, *Searching for signatures of E_6*, Phys. Rev. **D96** (2017) 015026, DOI: 10.1103/PhysRevD.96.015026, arXiv: 1607.06900 [hep-ph].

[11] F. del Aguila, M. Cvetic, P. Langacker, *Determination of Z-prime gauge couplings to quarks and leptons at future hadron colliders*, Phys. Rev. **D48** (1993) R969, DOI: 10.1103/PhysRevD.48.R969, arXiv: hep-ph/9303299 [hep-ph].

[12] G. Altarelli, B. Mele, M. Ruiz-Altaba, *Searching for New Heavy Vector Bosons in $p\bar{p}$ Colliders*, Z. Phys. **C45** (1989), [Erratum: Z. Phys.C47,676(1990)] 109, DOI: 10.1007/BF01552335, 10.1007/BF01556677.

[13] C. T. Hill, *Topcolor assisted technicolor*, Phys. Lett. **B345** (1995) 483, DOI: 10.1016/0370-2693(94)01660-5, arXiv: hep-ph/9411426 [hep-ph].

[14] N. Arkani-Hamed, A. G. Cohen, H. Georgi, *Electroweak symmetry breaking from dimensional deconstruction*, Phys. Lett. **B513** (2001) 232, DOI: 10.1016/S0370-2693(01)00741-9, arXiv: hep-ph/0105239 [hep-ph].

[15] R. Aaij et al., LHCb, *Test of lepton universality using $B^+ \to K^+ \ell^+ \ell^-$ decays*, Phys. Rev. Lett. **113** (2014) 151601, DOI: 10.1103/PhysRevLett.113.151601, arXiv: 1406.6482 [hep-ex].

[16] R. Aaij et al., LHCb, *Test of lepton universality with $B^0 \to K^{*0} \ell^+ \ell^-$ decays*, JHEP **08** (2017) 055, DOI: 10.1007/JHEP08(2017)055, arXiv: 1705.05802 [hep-ex].

[17] S. Bifani et al., *Review of Lepton Universality tests in B decays* (2018), arXiv: 1809.06229 [hep-ex].

[18] B. C. Allanach, B. Gripaios, T. You, *The case for future hadron colliders from $B \to K^{(*)} \mu^+ \mu^-$ decays*, JHEP **03** (2018) 021, DOI: 10.1007/JHEP03(2018)021, arXiv: 1710.06363 [hep-ph].

[19] U. Baur, I. Hinchliffe, D. Zeppenfeld, *Excited Quark Production at Hadron Colliders*, Int. J. Mod. Phys. **A2** (1987) 1285, DOI: 10.1142/S0217751X87000661.

[20] U. Baur, M. Spira, P. M. Zerwas, *Excited Quark and Lepton Production at Hadron Colliders*, Phys. Rev. **D42** (1990) 815, DOI: 10.1103/PhysRevD.42.815.

[21] R. M. Harris, K. Kousouris, *Searches for Dijet Resonances at Hadron Colliders*, Int. J. Mod. Phys. **A26** (2011) 5005, DOI: 10.1142/S0217751X11054905, arXiv: 1110.5302 [hep-ex].

[22] N. Boelaert, T. Akesson, *Dijet angular distributions at s**(1/2) =14-TeV*, Eur. Phys. J. **C66** (2010) 343, DOI: 10.1140/epjc/s10052-010-1268-8, arXiv: 0905.3961 [hep-ph].

[23] R. Sekhar Chivukula, E. H. Simmons, N. Vignaroli, *Distinguishing dijet resonances at the LHC*, Phys. Rev. **D91** (2015) 055019, DOI: 10.1103/PhysRevD.91.055019, arXiv: 1412.3094 [hep-ph].

[24] R. S. Chivukula et al., *Characterizing boosted dijet resonances with energy correlation functions*, JHEP **03** (2018) 133, DOI: 10.1007/JHEP03(2018)133, arXiv: 1710.04661 [hep-ph].

[25] L. Randall, R. Sundrum, *A Large mass hierarchy from a small extra dimension*, Phys. Rev. Lett. **83** (1999) 3370, DOI: 10.1103/PhysRevLett.83.3370, arXiv: hep-ph/9905221 [hep-ph].

[26] A. Pomarol, *Gauge bosons in a five-dimensional theory with localized gravity*, Phys. Lett. **B486** (2000) 153, DOI: 10.1016/S0370-2693(00)00737-1, arXiv: hep-ph/9911294 [hep-ph].

[27] H. Davoudiasl, J. L. Hewett, T. G. Rizzo, *Bulk gauge fields in the Randall-Sundrum model*, Phys. Lett. **B473** (2000) 43, DOI: 10.1016/S0370-2693(99)01430-6, arXiv: hep-ph/9911262 [hep-ph].

[28] Y. Grossman, M. Neubert, *Neutrino masses and mixings in nonfactorizable geometry*, Phys. Lett. **B474** (2000) 361, DOI: 10.1016/S0370-2693(00)00054-X, arXiv: hep-ph/9912408 [hep-ph].

[29] H. Davoudiasl, J. L. Hewett, T. G. Rizzo,
Experimental probes of localized gravity: On and off the wall, Phys. Rev. **D63** (2001) 075004,
DOI: 10.1103/PhysRevD.63.075004, arXiv: hep-ph/0006041 [hep-ph].

[30] T. Gherghetta, A. Pomarol, *Bulk fields and supersymmetry in a slice of AdS*,
Nucl. Phys. **B586** (2000) 141, DOI: 10.1016/S0550-3213(00)00392-8,
arXiv: hep-ph/0003129 [hep-ph].

[31] H. Davoudiasl, J. L. Hewett, T. G. Rizzo,
Phenomenology of the Randall-Sundrum Gauge Hierarchy Model,
Phys. Rev. Lett. **84** (2000) 2080, DOI: 10.1103/PhysRevLett.84.2080,
arXiv: hep-ph/9909255 [hep-ph].

[32] T. Sjï¿½strand et al., *An Introduction to PYTHIA 8.2*, Comput. Phys. Commun. **191** (2015) 159,
DOI: 10.1016/j.cpc.2015.01.024, arXiv: 1410.3012 [hep-ph].

[33] R. D. Ball et al., NNPDF, *Parton distributions for the LHC Run II*, JHEP **04** (2015) 040,
DOI: 10.1007/JHEP04(2015)040, arXiv: 1410.8849 [hep-ph].

[34] J. Alwall et al., *The automated computation of tree-level and next-to-leading order differential cross sections, and their matching to parton shower simulations*, JHEP **07** (2014) 079,
DOI: 10.1007/JHEP07(2014)079, arXiv: 1405.0301 [hep-ph].

[35] J. de Favereau et al., DELPHES 3,
DELPHES 3, A modular framework for fast simulation of a generic collider experiment,
JHEP **02** (2014) 057, DOI: 10.1007/JHEP02(2014)057, arXiv: 1307.6346 [hep-ex].

[36] M. Benedikt et al., *Future Circular Collider Study. Volume 3: The Hadron Collider (FCC-hh) Conceptual Design Report* (2018).

[37] *FCC-hh detector DELPHES card*, https://github.com/delphes/delphes/blob/master/cards/FCC/FCChh.tcl.

[38] S. Agostinelli et al., GEANT4, *GEANT4: A Simulation toolkit*,
Nucl. Instrum. Meth. **A506** (2003) 250, DOI: 10.1016/S0168-9002(03)01368-8.

[39] M. Cacciari, G. P. Salam, G. Soyez, *FastJet User Manual*, Eur. Phys. J. **C72** (2012) 1896,
DOI: 10.1140/epjc/s10052-012-1896-2, arXiv: 1111.6097 [hep-ph].

[40] M. Cacciari, G. P. Salam, G. Soyez, *The anti-k_t jet clustering algorithm*, JHEP **04** (2008) 063,
DOI: 10.1088/1126-6708/2008/04/063, arXiv: 0802.1189 [hep-ex].

[41] J. Thaler, K. Van Tilburg, *Identifying Boosted Objects with N-subjettiness*, JHEP **03** (2011) 015,
DOI: 10.1007/JHEP03(2011)015, arXiv: 1011.2268 [hep-ph].

[42] A. J. Larkoski et al., *Soft Drop*, JHEP **05** (2014) 146, DOI: 10.1007/JHEP05(2014)146,
arXiv: 1402.2657 [hep-ph].

[43] E. Perez Codina, P. G. Roloff, *Hit multiplicity approach to b-tagging in FCC-hh*,
tech. rep. CERN-ACC-2018-0023, Geneva: CERN, 2018,
URL: https://cds.cern.ch/record/2631478.

[44] E. Perez Codina, P. G. Roloff, *Tracking and Flavour Tagging at FCC-hh*,
tech. rep. CERN-ACC-2018-0027, Geneva: CERN, 2018,
URL: https://cds.cern.ch/record/2635893.

[45] T. Junk, *Confidence level computation for combining searches with small statistics*,
Nucl. Instrum. Meth. **A434** (1999) 435, DOI: 10.1016/S0168-9002(99)00498-2,
arXiv: hep-ex/9902006 [hep-ex].

[46] A. L. Read, *Presentation of search results: The CL(s) technique*, J. Phys. **G28** (2002), [,11(2002)] 2693, DOI: 10.1088/0954-3899/28/10/313.

[47] G. Cowan et al., *Asymptotic formulae for likelihood-based tests of new physics*, Eur. Phys. J. **C71** (2011), [Erratum: Eur. Phys. J.C73,2501(2013)] 1554, DOI: 10.1140/epjc/s10052-011-1554-0,10.1140/epjc/s10052-013-2501-z, arXiv: 1007.1727 [physics.data-an].

[48] V. Khachatryan et al., CMS, *Search for heavy resonances decaying to tau lepton pairs in proton-proton collisions at* $\sqrt{s} = 13$ *TeV*, JHEP **02** (2017) 048, DOI: 10.1007/JHEP02(2017)048, arXiv: 1611.06594 [hep-ex].

[49] A. J. Larkoski, F. Maltoni, M. Selvaggi, *Tracking down hyper-boosted top quarks*, JHEP **06** (2015) 032, DOI: 10.1007/JHEP06(2015)032, arXiv: 1503.03347 [hep-ph].